Electron-Electron Distances in Spin-Labeled Low-Spin Metmyoglobin Variants by Relaxation Enhancement

Dmitriy Ulyanov, Bruce E. Bowler, Gareth R. Eaton, and Sandra S. Eaton
Department of Chemistry and Biochemistry, University of Denver, Denver, Colorado 80208

ABSTRACT Thirteen single-cysteine variants of myoglobin were prepared by overexpression of apoprotein, spin labeling, and reconstitution with hemin. This procedure resulted in a protein with fewer hemichrome impurities than was obtained by an overexpression of holo-protein followed by spin labeling. Coordination of cyanide to the met heme formed low-spin complexes. Iron-nitroxyl interspin distances in the range of 17–30 Å were determined by saturation recovery measurements of the enhancement of the nitroxyl spin lattice relaxation rates between ~30–140 K, and by spin-echo measurements of the enhancement of spin-spin relaxation rates at 10–30 K. Interspin distances were also calculated, using the molecular modeling program Insight II (Accelrys, San Diego, CA). For most variants, distances determined from the temperature dependence of spin-echo intensities at a pulse spacing of 200 ns agree with distances measured by saturation recovery and calculated with Insight II within about an angstrom, which is within experimental uncertainties. Measurements of interspin distances via spin-spin relaxation enhancement have the advantages that maximum effects are observed for slower metal relaxation rates than are required for spin-lattice relaxation enhancement, and the impact diminishes as r^{-3} instead of r^{-6}, as with spin-lattice relaxation enhancement, which permits measurements at longer distances.

INTRODUCTION

Determination of distances between paramagnetic sites in proteins and polymers by electron paramagnetic resonance (EPR) can provide crucial structural constraints. Methods were developed to measure distances between paramagnetic centers from 5 up to ~70 Å (1). These techniques are all based on measuring electron-electron dipole-dipole interactions, and the method of choice for a particular system depends on the interspin distance and the relaxation rates of paramagnetic centers. Changes in continuous-wave (CW) lineshapes at shorter distances (2,3), and double-resonance double electron-electron resonance (4–6) or double-quantum coherence (7,8) at longer distances, can be used for pairs of slowly relaxing spins such as organic radicals, including nitroxyl spin labels. When one of the interacting spins is faster-relaxing, the relaxation rate of the more slowly relaxing spin is enhanced (9). Double-resonance methods of measuring interspin distances that are very powerful for pairs of organic radicals (5) are less useful for metal ions with EPR signals that extend over much wider ranges of magnetic fields. The enhancement of spin-lattice relaxation rates was used to determine distances between metals and radicals in photosystems (10,11), spin-labeled iron porphyrins and heme proteins (12–16), proteins containing iron-sulfur clusters (17–22), and the Cu_A site of cytochrome *c* oxidase and the iron in cytochrome *c* (23). Most of these studies were based on enhancements in spin-lattice (longitudinal) relaxation measured by saturation recovery, where the maximum impact on a slowly relaxing spin occurs when the metal relaxation rates are on the order of differences between the energies of the fast and slowly relaxing spins, or on the order of the EPR frequency. For many systems at *X*-band, this requires metal relaxation rates $>10^9\ s^{-1}$ (24). However, the maximum enhancement of spin-spin relaxation ($1/T_2$) occurs when the relaxation rate for the faster-relaxing center is on the order of the dipole-dipole interaction (in angular frequency units). For interspin distances of tens of angstroms, this only requires metal-relaxation rates on the order of $10^7\ s^{-1}$. The slower relaxation rates required for maximum impact on $1/T_2$ than on $1/T_1$ make it possible to use relaxation enhancement methods for metal centers with relaxation rates of $<10^9\ s^{-1}$ at accessible temperatures or at lower temperatures. The impact on $1/T_2$ diminishes as r^{-3} instead of r^{-6} for spin-lattice relaxation enhancement, which permits measurements at longer distances.

For spin-labeled heme porphyrins with interspin distances between 11–15 Å, it was shown that distances determined from CW lineshapes, from saturation recovery measurements of enhancement of spin-lattice relaxation, and from enhancement of spin-echo decay rates were in good agreement (12). Given the utility of distance measurements by relaxation enhancement, it is important to compare distances obtained by enhancement of spin-lattice and spin-spin relaxation for distances >15 Å. Myoglobin was selected as the protein for these studies, because of its extensive characterization by EPR and its relative stability.

Thirteen sites near the surface of sperm whale myoglobin (Fig. 1) were selected for mutation (MbH12C, MbA15C, MbA19C, MbA53C, MbK56C, MbA57C, MbV66C, MbK87C, MbQ91C, MbK98C, MbE148C, MbL149C, and MbG150C). Variants were chosen to sample distances and

Submitted July 8, 2008, and accepted for publication August 19, 2008.

Address reprint requests to Sandra S. Eaton, Department of Chemistry and Biochemistry, University of Denver, Denver, CO 80208-2436. Tel.: 303-871-3102; Fax: 303-871-2254; E-mail: Sandra.eaton@du.edu.

Editor: David D. Thomas.

0006-3495/08/12/5306/11 $2.00

doi: 10.1529/biophysj.108.141887

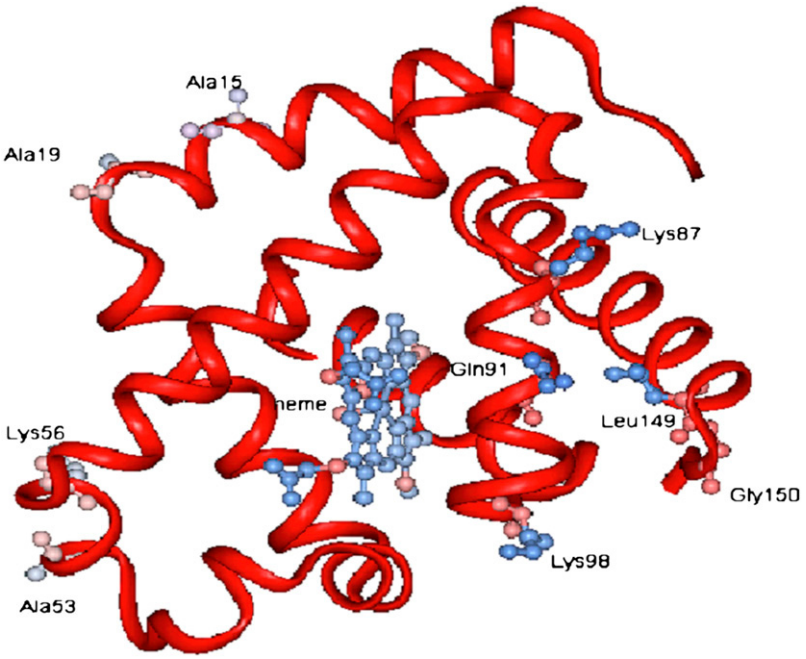

FIGURE 1 Ribbon diagram of sperm-whale myoglobin, based on Brookhaven Protein Database pdb1mbw file, showing nine native side chains that were replaced by cysteine mutations for attachment of spin labels.

orientations of the iron-nitroxyl interspin vector relative to the axes of the heme iron. Sites of mutations were selected that are not highly conserved (25) and do not participate in intramolecular hydrogen bonding (26–28). Sites with moderate solvent accessibility (29,30) were selected to facilitate spin-labeling without requiring protein-unfolding, and with the expectation that the probability of disrupting the structure would be lower than for buried sites (31). However, very high solvent accessibility can promote disulfide formation and protein dimerization in cysteine variants, which is undesirable. Most of the sites selected for mutation had solvent accessibilities between 40–85% (Table 1). Preliminary studies of interspin distances determined by spin-lattice relaxation enhancement for L-MbH12C-SL, L-MbA53C-SL, L-MbV66C-SL, and L-MbK98C-SL (L = CN^- or imidazole, SL = spin label) variants were reported (14). Cyanide was selected as the ligand in the studies reported here because the low-spin Fe(III) relaxation rates are faster for axial cyanide than for axial imidazole, resulting in greater enhancement of nitroxyl relaxation rates (14) at a given temperature.

TABLE 1 Characteristics of myoglobin sites selected for mutations

Variant	Solvent accessibility*	$\theta^{\dagger}$	$\phi^{\ddagger}$
MbK98C	76%	127	17
MbV66C	42%	50	23
MbK87C	68%	153	17
MbQ91C	47%	159	114
MbL149C	23%	149	102
MbG150C	79%	149	25
MbK56C	53%	10	7
MbE148C	70%	160	65
MbA57C	69%	26	71
MbA53C	90%	14	74
MbA19C	75%	43	47
MbA15C	70%	62	46
MbH12C	65%	63	77

*Calculated using the program ACCESS (29).
†Orientation of the Fe(III)-nitroxyl interspin vector relative to the z axis of the heme, calculated using Insight II.
‡Projection of the Fe(III)-nitroxyl interspin vector on the heme plane, relative to the heme Fe-N bond axis, calculated using Insight II.

EXPERIMENTAL SECTION

Preparation of myoglobin variants, Mb*X*, where *X* = one of 13 variants

The wild-type sperm-whale Mb synthetic gene in the pMb122 vector was a generous gift from the laboratory of S. G. Sligar (32,33). Except for the correction of Asn-122 to Asp-122 (33), the synthetic sperm-whale sequence obtained by Springer and Sligar (32) was used to prepare variants. The wild-type protein and several variants (MbH12C, MbA15C, MbA53C, MbV66C, MbK87C, and MbK98C) were previously constructed into the pBS(−) vector (Stratagene, La Jolla, CA) (14). These constructs were used as starting materials for introducing variant myoglobin genes into the pET-17b vector (Novagen, Madison, WI) (34), which was selected for overexpression of *apo*Mb*X* in inclusion bodies. Additional variants (MbA19C, MbK56C, MbA57C, MbQ91C, MbE148C, MbL149C, and MbG150C) were prepared using the QuikChange site-directed mutagenesis kit (Stratagene). The double-stranded supercoiled DNA of the pET-17b vector, containing wild-type myoglobin, was used as the template. Each variant was sequenced to confirm the presence of the desired mutation and no additional mutations.

The pET-17b vectors containing the Mb mutant genes were transformed into competent BL21(DE3) *Escherichia coli* host cells (Novagen). Cells were grown on LB/ampicillin media. The synthesis of recombinant *apo*Mb*X* was induced with isopropyl-β-D-thiogalactopyranoside. Cells were harvested by centrifugation and quickly frozen at −70° to facilitate subsequent lysis. Typical yields of wet cells were 3–5 g/L.

The apo protein predominantly occurred in inclusion bodies (IBs). Initially, protein purification and refolding used the procedure of Jennings et al.

(34). However, yields were low, so an alternate protocol based on CelLytic B Bacterial Cell Lysis Reagent (Sigma, St. Louis, MO) was developed. CelLytic B is a mild nonionic detergent that breaks up cells and permits the extraction of most soluble proteins. The manufacturer's protocol was followed, except that 2% sodium deoxycholate was substituted for the 1:10 diluted CelLytic B in the IB washing step. After isolation from cells, IBs were suspended in freshly prepared 8 M urea and 5 mM dithiothreitol (DTT), and stirred at 4°C for 2–4 h. The suspension was then centrifuged at 25,000 × *g* for 15 min, and the supernatant was retained. The concentration of *apo*Mb*X* was calculated based on $A_{280nm} = 14{,}800\ cm^{-1}\ M^{-1}$ in 8 M urea (35). The solution was diluted with fresh 8 M urea to $OD_{280nm} < 0.6$ (<0.8 mg *apo*Mb*X*/mL), to avoid precipitation in the subsequent refolding step (35). The protein was refolded by dialysis overnight at 4°C in ~8 L of 15 mM sodium acetate buffer, pH 7.0. Subsequent work with *apo*Mb*X* was performed at 4°C to avoid aggregation (36). The dialyzed protein solution was concentrated and centrifuged to remove residual debris. Proteins were judged to be more than 95% pure, based on sodium dodecyl sulfate gel electrophoresis.

Spin labeling of *apo*Mb*X* to make *apo*Mb*X*-SL, where *X* = one of 13 variants

Solutions of *apo*Mb*X* containing 10 mM DTT were shaken gently at 4°C for ~1 h to break any disulfide bonds. The DTT was removed with a PD-10 desalting column (Amersham Biosciences, now GE Life Sciences, Piscataway, NJ) equilibrated with 30 mM sodium phosphate buffer, pH 7.5 and used immediately for spin labeling. The concentration of *apo*Mb*X* was calculated based on $A_{280nm} = 15{,}800\ cm^{-1}\ M^{-1}$ (37). Then (1-oxyl-2,2,5,5-tetramethyl-Δ^3-pyrroline-3-methyl)methanethiosulfonate (MTSL, Toronto Research Chemicals, Inc., Toronto, Ontario, Canada) (7× excess, freshly dissolved in minimum volume of ethanol) was added, and the mixture was shaken gently overnight at 4°C. After concentrating the solution, excess MTSL was removed by passing though a PD-10 column equilibrated with 30 mM sodium phosphate buffer, pH 7.5. Quantitation of the CW nitroxyl EPR signal, by comparison of the double integral with standard solutions of tempol (4-hydroxy-2,2,6,6-tetramethylpiperidin-1-yl), indicated 90–100% spin-labeling efficiency. If not used immediately, the solution was flash-frozen in liquid nitrogen and stored at −70°C. The same procedure was used for all variants.

Reconstitution with Fe(III) heme to prepare CN-Mb*X*-SL, where *X* = one of 13 variants

Solutions of *apo*Mb*X*-SL were diluted to ~10 μM with 30 mM phosphate buffer, pH 7.5. A 1.1× molar excess of bovine hemin (Sigma) was dissolved in 50 μL of 1 M NaOH, diluted to 1 mM with 1:1 ethylene glycol/phosphate buffer (30 mM), and centrifuged to remove any undissolved solids (38). The hemin solution was added dropwise to the *apo*Mb solution in an ice bath, while maintaining pH below 9.0. The resulting solution was promptly concentrated to <1 mL by centrifuge ultrafiltration, and loaded on a G-50 superfine Sephadex size exclusion column (50 cm long, 1.5-cm diameter), equilibrated (and then eluted) with 20 mM TrisHCl and 1 mM EDTA, pH 8.4. Fractions with $A_{409nm}/A_{280nm} > 3$ were collected and concentrated. Yields for heme reconstitution were 40–95% for protein isolated using the deoxycholate wash of the IB. Lower yields of reconstituted protein were obtained if CelLytic was used in the washing step. The addition of CN^- to make CN-Mb*X*-SL was performed as described previously (14). Samples for EPR were prepared by the addition of an equal volume of glycerol, degassed, and frozen immediately in liquid nitrogen. Quantitation of ratios of high-spin and low-spin signals in the CW EPR spectra at ~15 K by integration and simulation (14) indicated 96–98% conversion to low-spin heme. Hemichrome is a general designation for degraded forms of the protein with altered axial ligation (39,40) that are difficult to detect by any method other than EPR spectroscopy at low temperatures. In some samples, hemichromes were observed and quantitated by simulation of the CW EPR spectra as a mixture of two species with different *g* values (14).

Reconstitution with Zn(II)porphyrin to make ZnMb*X*-SL, where *X* = one of six mutants

For six selected variants (MbA15C, MbK56C, MbK87C, MbK98C, MbL149C, and MbG150C), *apo*Mb*X*-SL was reconstituted with diamagnetic Zn(II) porphyrin, using a modification of a procedure in the literature (14). Zn(II)protoporphyrin IX (Aldrich Chemical Co., Milwaukee, WI), dissolved in a minimum volume of 0.1 M NaOH (~2 mg/mL), was centrifuged to remove undissolved solids. The solution was added dropwise to the solution of *apo*Mb*X*-SL, while maintaining pH below 10.0, followed by stirring overnight in the dark at 4°C. The pH was adjusted to 6.0 with 50 mM NaH_2PO_4, and the solution was loaded on a CM-Sephadex column equilibrated with 10 mM NaH_2PO_4. The ZnMb was eluted with a continuous gradient of NaCl from 0 to 0.5 M in 10 mM NaH_2PO_4, pH 6.0. Fractions with $A_{427nm}/A_{280nm} \geq 8$ were collected, concentrated, and exchanged into 20 mM TrisHCl, 1 mM EDTA, pH 8.4 buffer. Typical yields for reconstitution were 15–40%. Samples for EPR were prepared by the addition of an equal volume of glycerol, degassed by freeze-pump-thaw, and frozen immediately in liquid nitrogen. The Zn derivatives were used to measure spin-label relaxation rates in the absence of relaxation enhancement.

Measurements of interspin distances by saturation-recovery EPR

The spin-lattice relaxation rates for nitroxyl in ZnMb*X*-SL (where *X* = one of six variants) were measured by long-pulse saturation recovery (SR), as described previously (14), and were the same, within experimental uncertainty, for the six variants, and are similar to those of small-molecule nitroxyls (41). At lower temperatures, $1/T_1$ exhibited the T^2 dependence that is characteristic of the Raman process. At higher temperatures, relaxation rates were more strongly temperature-dependent, which is characteristic of a local mode. The temperature dependence of $1/T_1$ was modeled as the sum of these two contributions (42), which provided the fit function (Fig. 2) that was used to interpolate values required for the interspin-distance calculations. Relaxation rates for the low-spin Fe(III) in CN-Mb*X*-SL were determined by three-pulse inversion recovery between 7–15 K, and by analysis of the temperature-dependent contribution to the CW lineshapes at 35–60 K (14,43). Within experimental uncertainty, there was no difference in iron relaxation rates between variants, and spin-labeling of the protein had no impact on iron relaxation rates. The inversion recovery curves for low-spin Fe(III) were fit better with a distribution of exponentials than with a single exponential. Distributions of exponentials were also observed for spin-lattice relaxation rates of Cu(II) and vanadyl complexes (44,45), which is suggested to be a characteristic of transition metal complexes analogous to *g*-strain. The temperature dependence of relaxation rates for low-spin Fe(III) was modeled as the sum of contributions from the Raman process and a thermally activated process (14,46). The fit function (Fig. 2) was used to interpolate between 15–35 K, and to extrapolate above 60 K. The SR curves for nitroxyl interacting with low-spin heme Fe(III) were analyzed as reported previously (14), using the program MENOSR (12,24), which is based on the Bloembergen equation (47,48). At temperatures where Fe(III) relaxes quickly enough to impact nitroxyl relaxation significantly, T_1 is much faster than the T_m observed at lower temperatures, so it was assumed that T_2 was driven by T_1, and therefore that the iron $T_1 = T_2$. Values of interspin distance were calculated independently at 7–10 temperatures, and the averages are reported in Table 2. For samples that contained a measurable concentration of hemichrome (Table 2), its contribution to relaxation enhancement was included by assuming that the iron-relaxation rates in hemichrome are similar to those for bis-imidazole myoglobin (14). The inclusion of 6–10% hemichrome in the MENOSR calculations had a negligible impact on the calculated interspin distance. The sample with the highest concentration of hemichrome, CN-MbH12C-SL, also has an interspin distance of ~29 Å, so the observed relaxation enhancement is relatively small, and the presence of the hemichrome is not a large contribution to the uncertainty in the distance.

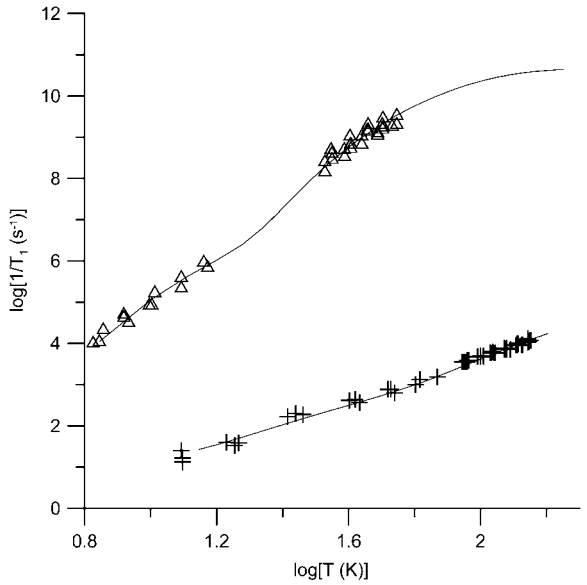

FIGURE 2 Temperature dependence of spin-lattice relaxation rates for nitroxyl in ZnMbX-SL (+) and for low-spin Fe(III) in several CN-Mb*X*-SL variants (Δ). Solid lines represent fit functions, based on models described in the text.

Measurement of interspin distances by electron spin echo EPR

Two pulse spin echoes were recorded on a Bruker E580 (Bruker BioSpin, Billerica, MA) with a split ring resonator and an Oxford 935 cryostat (Oxford Instruments, Oxford, UK). The resonator was over-coupled to Q ~100. Pulse lengths of 40 and 80 ns were used to record echo decays, to minimize the impact of proton modulation. To track trends in dephasing rates, a stretched exponential, Eq. 1, was fitted to the decays:

$$Y(\tau) = Y(0)\exp[-(2\tau/T_m)^x]. \quad (1)$$

The value of x was constrained to be >0.5 (49). The designation T_m is used to encompass all processes that contribute to echo dephasing, including T_2.

Relative echo intensities

Echo intensities at constant τ, measured with 40-ns and 80-ns pulses, were digitized with a Lecroy 9410 (LeCroy Corporation, Chestnut Ridge, NY) oscilloscope. These pulse lengths give a microwave B_1 of 2.4 Gauss, which is not large enough to encompass the complete dipolar splitting pattern at interspin distances of 18 Å ($2D = 9.6$ Gauss). The assumption was made that B_1 was large enough to sample the dipolar interactions present in the center of the nitroxyl spectrum. The shot repetition time was increased until the limiting echo intensity was observed. Echo intensities were multiplied by temperature to correct for the temperature dependence of Boltzmann populations. For each variant, echo intensity as a function of temperature was measured twice. Resonator Q was measured by the cavity ring-down method at 4.5 K, 15 K, and 75 K, and was found to vary by <10% over the time and temperatures required to acquire a data set.

In the Bruker Xepr software, the stored values for the time axis start at 0.0. To interpret the time evolution of the signal correctly, it is necessary to add the initial τ value to the stored values. In the Xepr software, pulse timing is described relative to the beginnings of the pulses, so $\tau = 400$ ns means that the time between the beginning of the first pulse and the beginning of the second pulse is 400 ns. The time between the start of the first pulse and the peak of the echo is 2τ + the average of the pulse lengths. Because the simulations do not attempt to account for the evolution of magnetization during pulses, we assumed it was best to define the time for the echo relative to the center of the second pulse. Therefore, half the width of the first pulse was added to the experimental values of τ, to permit comparisons with simulations.

Simulations

Simulations of the effects of Fe(III) on nitroxyl spin-echo dephasing were performed using the locally written program TMDYNAM (12,24). This program uses the equations of Zhidomirov and Salikhov (50) that describe spectral diffusion in a spin-coupled system. A limiting form of these expressions for the case where T_1 for the fast-relaxing center is short, relative to

TABLE 2 Point dipole interspin distances (Å) in spin-labeled, low-spin metmyoglobin variants

Variant	% hemichrome*	SR†	ESE at 200 ns‡	ESE at 500 ns‡	Insight II§
CN-MbK98C-SL	0	17.9 ± 0.3	17.9 ± 0.1	20.2 ± 0.3	16.9 ± 0.6
CN-MbV66C-SL	0	18.7 ± 0.7	18.2 ± 0.3	20.3 ± 0.3	19.0 ± 1.1
CN-MbK87C-SL	11¶	19.3 ± 0.3	18.5 ± 0.2	18.5 ± 0.2	18.8 ± 2.0
CN-MbQ91C-SL	0	19.7 ± 1.1	19.2 ± 0.7	23.8 ± 0.3	17.7 ± 1.1
CN-MbL149C-SL	14‖	22.4 ±1.4 or 16.8 and 25.5**	23.3 ± 0.2	27.4 ± 0.4	15.0 ± 2.0
CN-MbG150C-SL	0	22.8 ± 0.6 or 16.2 and 26.6**	23.6 ± 0.1	29.0 ± 0.1	21.9 ± 1.5
CN-MbK56C-SL	0	23.0 ± 0.9	23.6 ± 0.6	26.3 ± 0.6	23.1 ± 1.7
CN-MbE148C-SL	6¶	23.3 ± 0.6	23.2 ± 0.4	25.2 ± 1.2	24.5 ± 2.9
CN-MbA57C-SL	11¶	24.9 ± 0.8	22.8 ± 0.6	24.2 ± 1.2	28.0 ± 1.2
CN-MbA53C-SL	0	25.1 ± 1.1	25.8 ± 0.5	29.0 ± 0.2	26.6 ± 1.0
CN-MbA19C-SL	0	26.1 ± 0.8	27.2 ± 0.9	30.9 ± 0.3	27.7 ± 2.0
CN-MbA15C-SL	0	26.2 ± 1.4	26.2 ± 0.1	28.5 ± 0.1	24.1 ± 1.2
CN-MbH12C-SL	20¶	29.8 ± 0.7	27.8 ± 2.2	29.0 ± 2.5	30.0 ± 1.2

*Based on CW EPR spectra at 15 K, analyzed by simulation to determine relative populations.
†Uncertainties are based on measurements at 7–10 temperatures. Saturation recovery curves were analyzed assuming negligible distribution in interspin distances.
‡Uncertainty based on reproducibility of replicate measurements of echo intensity as a function of temperature.
§Uncertainties are based on range of conformations observed in thermal annealing calculations, sampling of geometries in canonical distribution, and range of conformations calculated with different solvation shells (14).
¶The g values at 15 K are $g_1 = \sim 3.08$–3.13, $g_2 = \sim 2.1$–2.2, and g_3 is poorly defined, similar to B hemichromes (54).
‖The g values at 15 K are $g_1 = 2.79$, $g_2 = 2.21$, and $g_3 = 1.73$, similar to H hemichromes (54).
**SR curves were fitted using two conformations with equal populations.

the dipolar splitting, is the leading term in the expressions by Kulikov and Likhtenshtein (48) for the impact of a rapidly relaxing spin on T_2 for a slowly relaxing spin (24). The TMDYNAM program has options to include Gaussian distributions in the metal-relaxation rate or in interspin distance. Because T_m for nitroxyls in ZnMb*X*-SL was independent of temperature between 10–70 K, it was assumed that in the absence of interaction with the rapidly relaxing Fe(III), T_m in CN-Mb*X*-SL would also be independent of temperature. In each sample of ZnMb*X*-SL or CN-Mb*X*-SL, the concentrations of protein and nitroxyl are essentially the same (see above), and are in the range of 0.3–1.0 mM. For higher-concentration samples and the 90° pulses used in the experiments, instantaneous diffusion contributed to echo dephasing (49,51), and the values of T_m obtained by fitting Eq. 1 to the spin-echo decay curves were concentration-dependent. Therefore, because the concentrations of ZnMb*X*-SL were different than for CN-Mb*X*-SL, the values of T_m in the absence of interaction with the rapidly relaxing Fe(III) were calculated for each sample from echo decays for CN-Mb*X*-SL at 6–8 K, where the Fe(III) is sufficiently slowly relaxing that both the relative echo intensity and the shape of the echo-decay curve are independent of temperature. Values of T_m at 7 K ranged from 3.3–4.1 μs, with values of x (Eq. 1) between 1.5–1.9. The observation of x at less than ~2.4 indicates a contribution from instantaneous diffusion or from the rotation of protein methyl groups in the vicinity of the nitroxyl (52). Relaxation rates for Fe(III) were calculated from the fit function shown in Fig. 2 at each temperature where TMDYNAM simulations were performed. Echo intensities were measured at the center of the nitroxyl spectrum, where there are contributions from many orientations of the molecule with respect to the external magnetic field. Orientation selection was taken into account in the simulations by including only those orientations of the molecule for which resonance was expected at the center field ± 5 Gauss. This bandwidth was selected to account for unresolved proton hyperfine coupling and the excitation bandwidth of pulses. For samples that contained a measurable concentration of hemichrome (Table 2), its contribution to relaxation enhancement was included by assuming that the iron-relaxation rates in hemichrome are similar to those for bis-imidazole myoglobin, which are slower than for cyanide adducts (14). Inclusion of the hemichrome contribution extends the temperature interval over which the echo intensity is near its minimum value, and decreases the estimated interspin distance.

RESULTS AND DISCUSSION

The locations of the heme and of nine mutations selected for study are shown in the ribbon diagram for sperm-whale myoglobin in Fig. 1. Locations were selected to sample regions of the protein with differing orientations of the electron-electron interspin vector relative to the magnetic axes of heme Fe(III) (Table 1). In previous studies of interspin distances in spin-labeled met-myoglobin, variants were prepared by overexpressing the holo heme protein and subsequent spin-labeling (14). It was observed that most variants were less stable than wild-type myoglobin, and for some variants, substantial amounts of hemichrome were formed during the time required for protein isolation and spin-labeling (14). Based on the g values, the hemichromes in CN-MbH12C-SL, CN-MbA57C-SL, CN-MbK87C-SL, and CN-MbE148C-SL were assigned as B-type or H-type bis-histidyl-ligated (53,54). The presence of significant quantities of hemichrome in a sample complicates the interpretation of relaxation enhancement, because cyanide ion does not bind well to hemichrome, and the iron-relaxation rates are slower for bis-imidazole-ligated low-spin heme than for cyanide adducts (14). Because the extent of hemichrome formation increased with sample-handling time, an alternate approach was taken to prepare the variants for this study. The mutant apoproteins were prepared and spin-labeled before introduction of the heme iron. This approach made it possible to prepare most of the variants with negligible amounts of hemichrome (Table 2). Even the relatively unstable CN-MbH12C-SL variant was prepared with only 20% hemichrome, which is much lower than previous attempts to prepare it from overexpressed holoprotein (14). The low stability of the MbH12C mutation was not anticipated based on a previous examination of the structure, but may be related to the report of unexpected instability for an L11A mutation (55). This low stability may also be related to the proposal that H12 is a stabilizing residue in whale globins (56), which is consistent with the long-range interaction between H12 and Asp-122 that can be seen in the x-ray structure of metaquoMb (57).

The conformations of spin-labeled proteins were calculated using Insight II software (Accelrys, San Diego, CA), as previously reported (14). The interspin distances reported for Insight calculations (Table 2) are the averages for conformations obtained by thermal annealing, for samplings from canonical distributions, and for solvent shells composed of water or glycerol (14). The standard deviations of calculated interspin distances of 1–2 Å indicate that even with thermal annealing and a variety of solvent shells, the changes in calculated conformations were relatively modest. There are inherent uncertainties in the calculations, but these values of r are more appropriate for comparisons with the experimental point-dipole values obtained by the EPR experiments than are the distances from the metal to the β-carbons of mutation sites that can be obtained from the x-ray structures of the wild-type protein.

Distances calculated by SR

Examples of SR curves and simulations are shown in Fig. 3 (CN-MbK87C-SL) and Fig. 4 (CN-MbA53C-SL). The maximum effect of iron on nitroxyl relaxation occurred between ~40–110 K, where iron-relaxation rates are on the order of 5×10^8 to 3×10^{10} (Fig. 2). Simulations of SR curves were performed with the locally written program MENOSR (12). The g values for low-spin Fe(III) were taken from simulations of CW spectra. At each temperature, T_1 for nitroxyl in the absence of interaction with rapidly relaxing iron and T_1 for low-spin Fe(III) were calculated from the corresponding fit functions for temperature dependence (Fig. 2), and were used as inputs for calculation of the SR curve. In Figs. 3 and 4, dashed lines denote the SR curve predicted for this value of T_1. Simulations were done first for the orientation of the interspin vector calculated using Insight II (Table 1). Values of r were adjusted to give the best fit to the experimental data. When the angles that defined the orientation of the interspin vector were varied, the best-fit value of r varied by up to 1.5 Å. The shapes of SR curves were not sufficiently dependent on the orientation of the interspin vector to define a best-fit orientation.

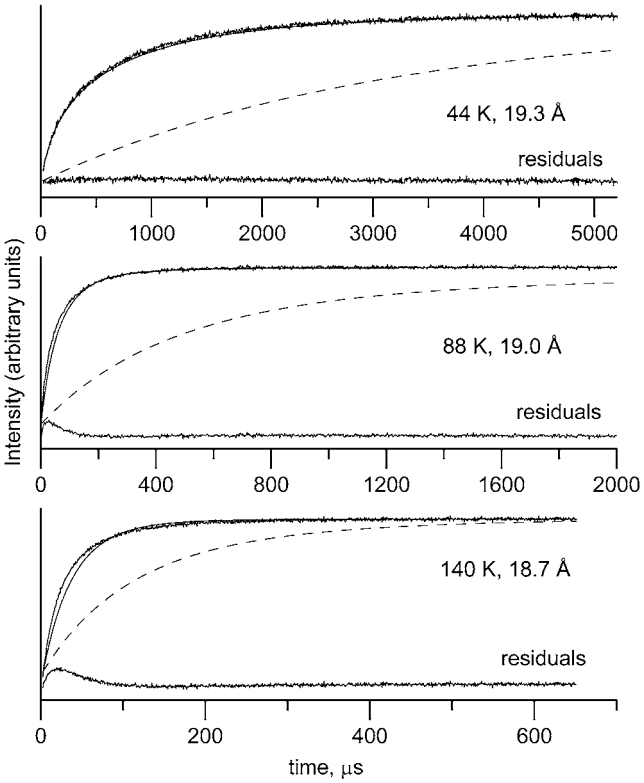

FIGURE 3 Saturation-recovery curves for nitroxyl in CN-MbK87C-SL at 44 K, 88 K, and 140 K. Noise-free solid lines are fits to experimental data calculated using MENOSR, which is based on the Bloembergen equation (see text). Dashed lines are curves predicted for ZnMb*X*-SL at each temperature, based on the fit function shown in Fig. 2. Residuals are plotted on the same scale. Note the large changes in the *x* axes with temperature.

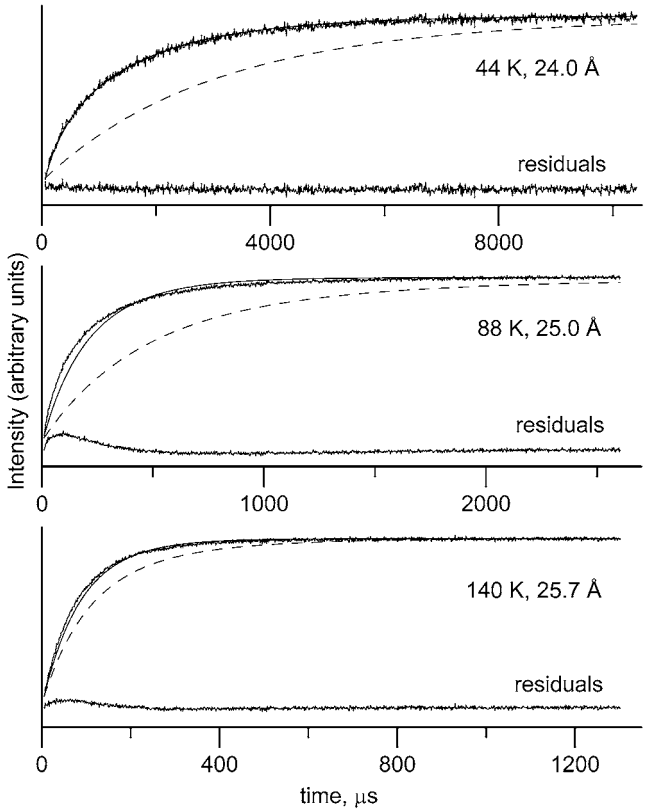

FIGURE 4 Saturation-recovery curves for nitroxyl in CN-MbA53C-SL at 44 K, 88 K, and 140 K. Noise-free solid lines are fits to experimental data calculated using MENOSR, which is based on the Bloembergen equation (see text). Dashed lines are curves predicted for ZnMb*X*-SL at each temperature, based on the fit function shown in Fig. 2. Residuals are plotted on same scale. Note the large changes in the *x* axes with temperature.

Values of *r* in Table 2 are averages calculated for SR curves at 7–10 temperatures where the relaxation enhancement, estimated by fitting a single exponential to the SR data, was at least 15%. The recovery curve for CN-MbA53C-SL at 140 K (Fig. 4) is an example of enhancement by only ~15%. The inclusion of distributions of low-spin Fe(III) T_1 values in the MENOSR calculations did not significantly improve the fits to the experimental SR curves. For most variants, the inclusion of a distribution of values of *r* also did not significantly improve the fit to the experimental data. However, for CN-MbL149C-SL and CN-MbG150C-SL, which are near the C-terminus of the amino-acid chain, the fits to the SR curves were better for a model that assumed two conformations with interspin distances that differed by ~8 Å. Two nitroxyl conformations for which the positions of the N-O group differed by about this amount were reported for spin-labeled T4 lysozyme (58).

Distances calculated by electron spin echo

For ZnMb*X*-SL, the shapes of echo-decay curves were independent of temperature between ~6–70 K. A stretched exponential (Eq. 1) gave good fits to the curves, with *x* in the range of 1.5–1.9, as expected when echo dephasing is dominated by proton-spin diffusion (49,52), but with some contribution from instantaneous diffusion. However, for CN-Mb*X*-SL, the echo-decay curves were strongly temperature-dependent (Fig. 5). When a stretched exponential (Eq. 1) was fitted to the decays, the values of T_m were strongly temperature-dependent (Fig. 5), and values of *x* changed from ~2 at low temperature to ~0.5 near 20 K, and back to ~1.0 at higher temperatures. These changes in T_m and *x* are characteristic of a system in a temperature range in which a dynamic process that averages inequivalent EPR signals goes from slow to intermediate to fast on the EPR time scale (59). In spin-coupled systems, the dynamic process is electron spin relaxation, and the inequivalence is the splitting of the signal for the nitroxyl due to dipolar coupling to the metal center (24). The shorter the interspin distance, the greater the maximum enhancement in $1/T_m$.

Simulations

The locally written program TMDYNAM (12,60) was used to simulate the echo-decay curves for CN-Mb*X*-SL as a

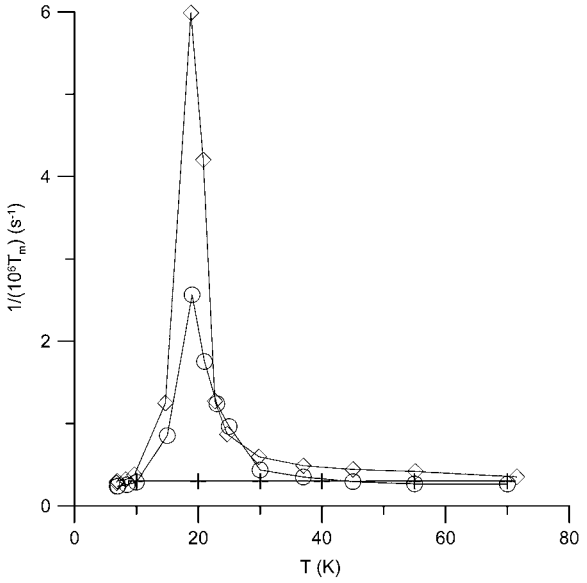

FIGURE 5 Temperature dependence of nitroxyl spin-echo dephasing rates for ZnMbA15C-SL (+), CN-MbA19C-SL (O), and CN-MbK87C-SL (◇). Echo-decay curves at the center of nitroxyl spectrum were fitted with a stretched exponential (Eq. 1), with the constraint that the minimum exponent was 0.5. Solid lines connect the data points.

function of temperature. Curves for CN-MbV66C-SL and simulations calculated for $r = 18.0$ Å are shown in Fig. 6. These results are typical of what was observed for all variants: the agreement between experiment and calculated echo-decay curves was better below ~30 K than at higher temperatures. The simulated curves are sums of powder distributions of orientations of molecules with respect to the external field. The

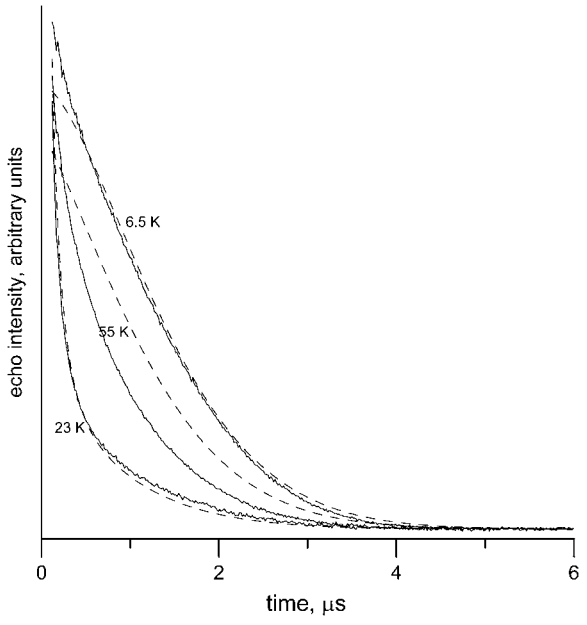

FIGURE 6 Spin-echo decay curves for the nitroxyl signal in CN-MbV66C-SL at 6.5 K, 23 K, and 55 K. Dashed lines are simulations calculated using TMDYNAM, $r = 18.0$ Å, as described in the text.

dipolar interaction depends on the orientation of the interspin vector relative to the external field, so the calculated echo-decay curves are the sum of contributions from molecules with different magnitudes of dipolar interaction. At lower temperatures, the impact of iron on nitroxyl echo dephasing depends only on the metal-relaxation rate, and is independent of the magnitude of spin-spin interaction, so the decay is a single exponential. When the metal-relaxation rate becomes comparable to the dipolar interaction (in angular frequency units), maximum relaxation enhancement is observed, and the shape of the echo-decay curve depends on the magnitude of splitting. As the metal-relaxation rate increases further, the relaxation enhancement decreases, the shape of the decay curve depends on the square of the dipolar coupling (24), and the echo decays are not single exponentials. The poorer agreement between calculated and experimental echo-decay curves at higher temperatures indicates either that 1), the dependence of the echo-dephasing rate on the magnitude of dipolar coupling was not adequately taken into account, or 2), there are additional contributions to echo-dephasing that were not adequately accounted for in the simulations.

Rather than analyzing the full shapes of echo-decay curves as a function of temperature, it is more convenient to determine interspin distance by analyzing echo intensity as a function of temperature at constant τ (24). To correct for changes in Boltzmann populations, the relative echo intensity is calculated by multiplying the absolute echo intensity by temperature. Plots of relative echo intensity as a function of temperature for two variants are shown in Fig. 7. The minimum echo intensity is observed at ~22 K, where the iron-relaxation rate is comparable to the average dipolar coupling. The minimum echo intensity is smaller for variants with shorter interspin distances, and for $\tau = 500$ ns than for $\tau = 200$ ns. The solid lines connect values of relative echo intensity calculated at temperatures where experimental data were obtained. In the simulations, the value of r was adjusted to match the relative echo intensities at minimum values of either $\tau = 200$ ns or 500 ns. The shapes of plots of calculated values were in better agreement with the experimental plots for a distribution of iron-relaxation rates than for single values. The plots in Fig. 7 and the interspin distances listed in Table 2 were calculated with a distribution width equal to the value of T_1, which is consistent with the inversion recovery curves for the iron signal at low temperatures. Distributions in r did not improve the match between the calculated and experimental temperature dependence of relative echo intensity.

The agreement between experimental and calculated values of relative echo intensity as a function of temperature is better below ~25 K than at higher temperatures, paralleling the trends in quality of fit to the echo-decay curve. At 40–60 K, the disagreement between calculated and experimental echo intensities decreased systematically with increasing interspin distance, and was greater for $\tau = 500$ ns than for $\tau = 200$ ns (Fig. 7). On average, interspin distances calculated from an analysis of echo intensities at $\tau = 500$ ns

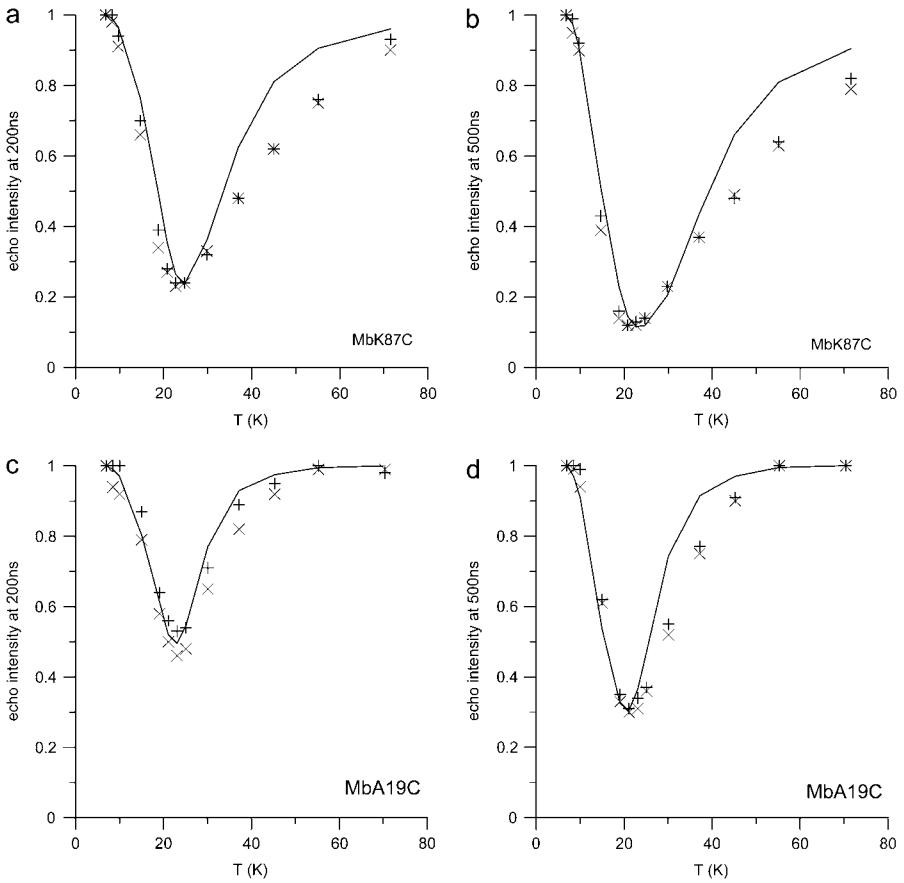

FIGURE 7 Temperature dependence of relative echo intensity, corrected for temperature dependence of Boltzmann populations. Data points for replicate data sets are shown as + and *x*. Solid lines connect points calculated using TMDYNAM at temperatures for which experimental intensities were recorded. (*a*) CN-MbK87C-SL, $\tau = 200$ ns, simulated with $r = 18.5$ Å. (*b*) CN-MbK87C-SL, $\tau = 500$ ns, simulated with $r = 18.5$ Å. (*c*) CN-MbA19C-SL, $\tau = 200$ ns, simulated with $r = 27.2$ Å. (*d*) CN-MbA19C-SL, $\tau = 500$ ns, simulated with $r = 30.9$ Å.

were 2.7 Å longer than those obtained at $\tau = 200$ ns, and the range of discrepancies was 0–5.4 Å. Two of the largest discrepancies between distances calculated from data at $\tau = 200$ ns and 500 ns were for CN-MbL149C-SL and CN-MbG150C-SL, which are sites for which the SR data suggested the presence of two conformations with distinctly different iron-nitroxyl distances.

Comparison of distances obtained by SR and electron spin echo

Iron-nitroxyl interspin distances between ~17–30 Å were examined, including the greatest distances that could be achieved with a protein of this size. The interspin distances determined by SR and by electron spin echo (ESE) at $\tau = 200$ ns agree within about 1 Å or less (Table 2), which is within experimental uncertainties, except for CN-MbA57C-SL, where the difference is ~2 Å. The largest differences between distances determined by SR or ESE and by molecular modeling (Fig. 8, *a* and *b*) were for CN-MbL149C-SL and CN-MbA57C-SL. For both CN-MbL149C-SL and CN-MbG150C-SL, the SR curves fit better to a sum of contributions with approximately equal weightings and interspin distances that differed by ~8 Å, than for a single conformation. Simulations of the temperature dependence of relative echo intensity were about the same for an average distance or for the sum of equal populations of two conformations with different distances. Crystal structures of several spin-labeled T4 lysozyme variants exhibited differences in conformations of nitroxyl (58) that could cause changes in interspin distances of this magnitude. Variations of side-chain conformations are not surprising (61), because MbL149 and MbG150 are at the C-terminal end of the myoglobin peptide chain and at the end of a helix. Hydrogen-exchange (62) and sulfide-exchange (63) studies showed that the segment containing MbL149 and MbG150 is quite flexible. The leucine at position 149 is a nonpolar residue, and has lower solvent accessibility than other sites examined in these studies (Table 1). Examination of the crystal structure data shows that Leu-149 is pointed toward side chains on the adjacent helix. Insertion of a more polar spin label at this location may result in less well-defined conformations of nitroxyl than at other locations in the protein. The conformations sampled in molecular modeling calculations for CN-MbL149C-SL are similar to the shorter-distance conformations estimated from SR curves. For CN-MbG150C-SL, molecular-modeling calculations gave distances near the average values obtained by ESE and SR. The differences in values of r obtained by ESE, SR, and molecular modeling for CN-MbA57C-SL suggest that several conformations may also be present for this variant. Ala-57 is also in a region of the protein where hydrogen-exchange studies found flexibility (62).

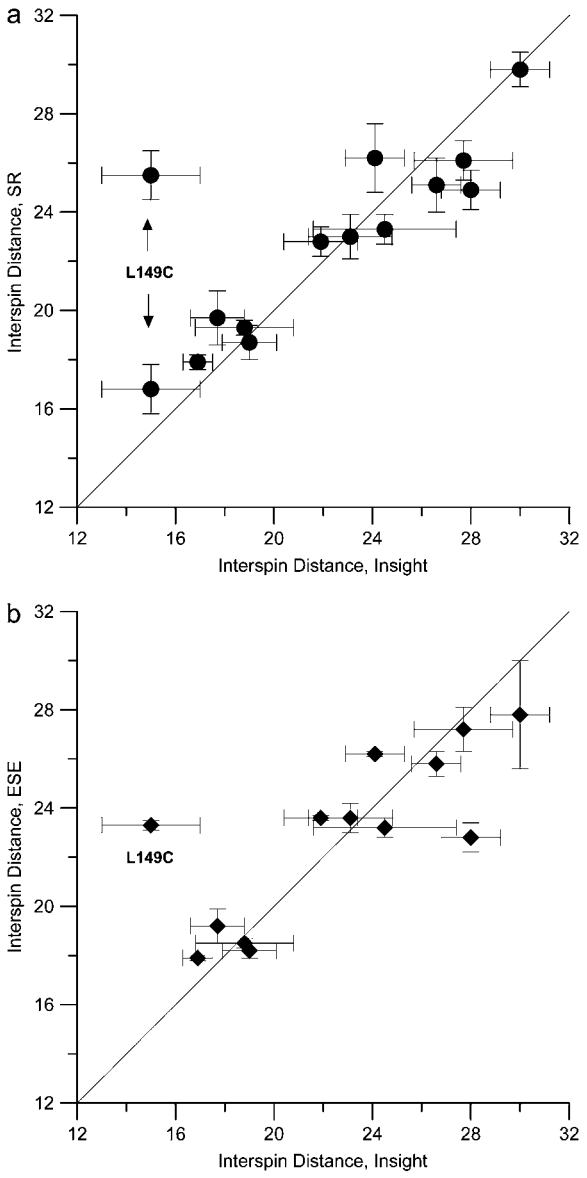

FIGURE 8 (*a*) Correlation between iron-nitroxyl distances (Å) calculated with Insight II and determined by saturation recovery. For CN-MbL149C-SL, points for both conformations found by fitting SR curves are shown. (*b*) Correlation between iron-nitroxyl distances (Å) calculated with Insight II and determined by electron spin echo with interpulse spacing $\tau = 200$ ns. For CN-MbL149C-SL, the average distance is shown. Solid lines with a slope of 1 show where points would fall if the correlations were perfect.

Factors that might contribute to discrepancies in distances determined by ESE

In spin-echo experiments, the interspin distances calculated based on the temperature dependence of relative echo intensities at pulse spacings of 500 ns were greater than those obtained for pulse spacings of 200 ns or from SR experiments. Simulations showed that systematic errors in metal-relaxation rates could shift the maximum relaxation enhancement to higher or lower temperatures, but did not change the magnitude of maximum enhancement, so systematic errors in iron-relaxation times would not account for the discrepancy in distances. The selection of the value of r to fit the echo-intensity data is based primarily on intensities at ~20 K, where relaxation enhancement is greatest (Fig. 7). The need to use longer distances to match the experimental intensities indicates that the model overestimates the impact on echo dephasing in this regime, where the iron-relaxation rate is comparable to the dipolar coupling. Between ~40–60 K, the experimental decay rates are faster than predicted, and the relative echo intensities are more perturbed than predicted, suggesting that the model underestimates relaxation enhancement. These discrepancies between 40–60 K suggest an additional distance-dependent contribution to enhanced relaxation, with significant contributions only at higher temperatures.

When the dipolar-interaction Hamiltonian is factored into terms designated by the letters *A–F* (64), the term identified as *A* is the basis for calculations of enhanced spin-echo dephasing, using TMDYNAM. The term *A* does not contribute to the enhancement of spin-lattice relaxation. The terms *B* and *C* make contributions of comparable magnitude to the enhancement of spin-lattice relaxation and spin-echo dephasing. In the 40–60 K range, relaxation enhancements from terms *B* and *C* that are significant relative to values of T_1 on the order of hundreds of microseconds are insignificant relative to T_m values on the order of 1 μs, and so are not included in TMDYNAM. Further work is needed to evaluate other possible sources of relaxation enhancements.

Distance ranges for enhancement effects

For measurements of interspin distances by spin-lattice relaxation enhancement in these low-spin heme systems, 30 Å, as in CN-MbH12C-SL, is about the upper limit. However, the relaxation enhancement of $1/T_2$ falls off less rapidly with increasing interspin distance than the enhancement of $1/T_1$. The impact of low-spin Fe(III) on relative echo intensity at 20 K for CN-MbH12C-SL ($r = 30$ Å) is ~0.6 for $\tau = 200$ ns and ~0.4 at $\tau = 500$ ns, which indicates that significant effects of Fe(III) on nitroxyl echo intensity could be measured for distances that are substantially longer than 30 Å. This comparison indicates that for the same iron center, enhancements of spin-echo dephasing can be useful at longer distances than enhancements of spin-lattice relaxation.

CONCLUSIONS

Thirteen variants of myoglobin were prepared by overexpression and spin-labeling of the apo protein before reconstitution with hemin. For less stable variants, this procedure produces protein with less hemichrome than is obtained by expression of the holo-protein with subsequent spin labeling. For most variants, distances in the range of 17–30 Å obtained by SR and from the temperature dependence of relative echo intensities measured with an interpulse spacing of 200 ns agreed well with distances obtained by calculations using the

Insight II molecular-modeling program. The poorer agreement for longer interpulse spacings, and for the shapes of echo-decay curves at temperatures above ~30 K, indicates that the current model for enhancement of spin-echo decays is not sufficient to explain all aspects of the data. Mutants at the C-terminus (L149 and G150) appear to have less well-defined conformations of nitroxyl than at other locations in the protein.

The support of this work by National Institutes of Health grant NIBIB EB002807 is gratefully acknowledged.

REFERENCES

1. Berliner, L. J., G. R. Eaton, and S. S. Eaton, editors. 2000. Biological Magnetic Resonance, Volume 19: Distance Measurements in Biological Systems by EPR. Kluwer Academic: New York.
2. Rabenstein, M. D., and Y.-K. Shin. 1995. Determination of the distance between two spin labels attached to a macromolecule. *Proc. Natl. Acad. Sci. USA*. 92:8239–8243.
3. Hustedt, E. J., A. I. Smirnov, C. F. Laub, C. E. Cobb, and A. H. Beth. 1997. Molecular distances from dipolar coupled spin-labels: the global analysis of multifrequency continuous wave electron paramagnetic resonance data. *Biophys. J.* 72:1861–1877.
4. Jeschke, G. 2002. Distance measurements in the nanometer range by pulse EPR. *Chem. Phys. Chem.* 3:927–932.
5. Jeschke, G., M. Pannier, and H. W. Spiess. 2000. Double electron-electron resonance. *Biol. Magn. Reson.* 19:493–512.
6. Tsvetkov, Y. D., and A. D. Milov. 2002. Pulsed ESR double resonance (PELDOR) spectroscopy: applications to spin-labeled peptides. *In* EPR in the 21st Century: Basics and Applications to Material, Life, and Earth Sciences. A. Kawamori, J. Yamauchi, and H. Ohta, editors. Elsevier, Amsterdam. 647–658.
7. Borbat, P. P., and J. H. Freed. 2000. Double-quantum ESR and distance measurements. *Biol. Magn. Reson.* 19:383–459.
8. Chiang, Y.-W., P. P. Borbat, and J. H. Freed. 2005. The determination of pair distance distributions by pulsed ESR using Tikhonov regularization. *J. Magn. Reson.* 172:279–295.
9. Bloembergen, N., E. M. Purcell, and R. V. Pound. 1948. Relaxation effects in nuclear resonance absorption. *Phys. Rev.* 73:679–712.
10. Lakshmi, K. V., and G. W. Brudvig. 2001. Pulsed electron paramagnetic resonance methods for macromolecular structure determination. *Curr. Opin. Struct. Biol.* 11:523–531.
11. Likhtenshtein, G. I. 2000. Depth of immersion of paramagnetic centers in biological systems. *Biol. Magn. Reson.* 19:309–346.
12. Rakowsky, M. H., K. M. More, A. V. Kulikov, G. R. Eaton, and S. S. Eaton. 1995. Time-domain electron paramagnetic resonance as a probe of electron-electron spin-spin interaction in spin-labeled low-spin iron porphyrins. *J. Am. Chem. Soc.* 117:2049–2057.
13. Zhou, Y., B. E. Bowler, G. R. Eaton, and S. S. Eaton. 2000. Electron spin-lattice relaxation rates for high-spin Fe(III) complexes in glassy solvents at temperatures between 6 and 298 K. *J. Magn. Reson.* 144:115–122.
14. Zhou, Y., B. E. Bowler, K. Lynch, S. S. Eaton, and G. R. Eaton. 2000. Interspin distances in spin-labeled metmyoglobin variants determined by saturation recovery EPR. *Biophys. J.* 79:1039–1052.
15. Budker, V., J.-L. Du, M. Seiter, G. R. Eaton, and S. S. Eaton. 1995. Electron-electron spin-spin interaction in spin-labeled low-spin methemoglobin. *Biophys. J.* 68:2531–2542.
16. Seiter, M., V. Budker, J.-L. Du, G. R. Eaton, and S. S. Eaton. 1998. Interspin distances determined by time domain EPR of spin-labeled high-spin methemoglobin. *Inorg. Chim. Acta*. 273:354–366.
17. Fournel, A., S. Gambarelli, B. Guigliarelli, C. More, M. Asso, G. Chouteau, R. Hille, and P. Bertrand. 1998. Magnetic interactions between a $[4Fe\text{-}4S]^{+}$ cluster and a flavin mononucleotide radical in the enzyme trimethylamine dehydrogenase: a high-field electron paramagnetic resonance study. *J. Chem. Phys.* 109:10905–10913.
18. Guigliarelli, B., C. More, A. Fournel, M. Asso, E. C. Hatchikian, R. Williams, R. Cammack, and P. Bertrand. 1995. Structural organization of the Ni and (4Fe-4S) centers in the active form of *Desulfovibrio gigas* hydrogenase. Analysis of the magnetic interactions by electron paramagnetic resonance spectroscopy. *Biochemistry*. 34:4781–4790.
19. Stevenson, R. C., W. R. Dunham, R. H. Sands, T. P. Singer, and H. Beinert. 1986. Studies on the spin-spin interaction between flavin and iron-sulfur cluster in an iron-sulfur flavoprotein. *Biochim. Biophys. Acta*. 869:81–88.
20. Vinogradov, A. D., V. D. Sled, D. S. Burbaev, V. G. Grivennikova, I. A. Moroz, and T. Ohnishi. 1995. Energy-dependent complex I-associated ubisemiquinones in submitochondrial particles. *FEBS Lett.* 370:83–87.
21. Fielding, A. J., R. J. Usselman, N. Watmough, M. Simkovic, F. E. Frerman, G. R. Eaton, and S. S. Eaton. 2008. Electron paramagnetic resonance characterization and interspin distance measurement of electron transfer flavoprotein ubiquinone oxidoreductase (ETF-QO). *J. Magn. Reson.* 190:222–232.
22. Usselman, R. J., A. J. Fielding, F. E. Frerman, G. R. Eaton, and S. S. Eaton. 2008. Impact of mutations on the midpoint potential of the $[4Fe\text{-}4S]^{+}$ cluster and on the catalytic activity in electron transfer flavoprotein-ubiquinone oxidoreductase (ETF-QO). *Biochemistry*. 47:92–100.
23. Lyubenova, S., M. K. Siddiqui, M. J. M. Penning DeVries, B. Ludwig, and T. F. Prisner. 2007. Protein-protein interactions studied by EPR relaxation measurements: cytochrome *c* and cytochrome *c* oxidase. *J. Phys. Chem. B*. 111:3839–3846.
24. Eaton, S. S., and G. R. Eaton. 2000. Determination of distances based on T_1 and T_m effects. *Biol. Magn. Reson.* 19:347–381.
25. Suzuki, T., and K. Imai. 1998. Evolution of myoglobin. *Cell. Mol. Life Sci.* 54:979–1004.
26. Takano, T. 1977. Structure of myoglobin refined at 2.0 Å resolution. II. Structure of deoxymyoglobin from sperm whale. *J. Mol. Biol.* 110: 569–584.
27. Takano, T. 1977. Structure of myoglobin refined to 2.0 Å resolution. I. Crystallographic refinement of metmyoglobin from sperm whale. *J. Mol. Biol.* 110:537–568.
28. Maurus, R., R. Bogumil, N. T. Nguyen, A. G. Mauk, and G. Brayer. 1998. Structural and spectroscopic studies of azide complexes of horse heart myoglobin and the His-64 to Thr variant. *Biochem. J.* 332:67–74.
29. Lee, B., and F. M. Richards. 1971. The interpretation of protein structures: estimation of static accessibility. *J. Mol. Biol.* 55:379–400.
30. Bowler, B. E., K. May, T. Zaragoza, P. York, A. Dong, and W. S. Caughey. 1993. Destabilizing effects of replacing a surface lysine of cytochrome *c* with aromatic amino acids: implications for the denatured state. *Biochemistry*. 32:183–187.
31. Alber, T. S., S. Dao-pin, J. A. Nye, D. C. Muchmore, and B. W. Matthews. 1987. Temperature-sensitive mutations of bacteriophage T4 lysozyme occur at sites with low mobility and low solvent accessibility in the folded protein. *Biochemistry*. 26:3754–3758.
32. Springer, B. A., and S. G. Sligar. 1987. High-level expression of sperm whale myoglobin in *Escherichia coli*. *Proc. Natl. Acad. Sci. USA*. 84: 8961–8965.
33. Phillips, G. N., Jr., R. M. Arduini, B. A. Springer, and S. G. Sligar. 1990. Crystal structure of myoglobin from a synthetic gene. *Proteins Struct. Funct. Genet.* 7:358–365.
34. Jennings, P. A., M. J. Stone, and P. E. Wright. 1995. Overexpression of myoglobin and assignment of its amide, Cα and Cβ resonances. *J. Biomol. NMR*. 6:271–276.
35. DeYoung, L. R., K. A. Dill, and A. L. Fink. 1993. Aggregation and denaturation of apomyoglobin in aqueous urea solutions. *Biochemistry*. 32:3877–3886.
36. Rossi-Fanelli, A., E. Antonini, and A. Caputo. 1958. Pure native globin from human hemoglobin: preparation and some physico-chemical properties. *Biochim. Biophys. Acta*. 28:221.

37. Stryer, L. 1965. The interaction of a naphthalene dye with apomyoglobin and apohemoglobin. A fluorescent probe of nonpolar binding sites. *J. Mol. Biol.* 13:482–495.

38. Smith, M. H. 1959. Kinetics and equilibria in systems containing heme, carbon monoxide, and pyridine. *Biochem. J.* 73:90–101.

39. Peisach, J., and W. E. Blumberg. 1971. Specific compounds formed during the reversible and irreversible denaturation of hemoglobin and its constituent chains. *Genet., Funct., Phys. Stud. Hemoglobins, Proc. 1st Inter-Amer. Symp. Hemoglobins*. 199–207.

40. DiIorio, E. 1981. Hemoglobins. *Methods Enzymol.* 76:57–72.

41. Sato, H., V. Kathirvelu, A. J. Fielding, S. E. Bottle, J. P. Blinco, A. S. Micallef, S. S. Eaton, and G. R. Eaton. 2007. Impact of molecular size on electron spin relaxation rates of nitroxyl radicals in glassy solvents between 100 and 300 K. *Mol. Phys.* 105:2137–2151.

42. Zhou, Y., R. Mitri, G. R. Eaton, and S. S. Eaton. 1999. Electron spin lattice relaxation processes for molecular $S = 1/2$ systems in glassy matrices at temperatures between 10 and 130 K. *Curr.Top. Biophys.* 23:63–68.

43. Rakowsky, M. H., G. R. Eaton, and S. S. Eaton. 1998. Comparison of the effect of high-spin and low-spin Fe(III) on nitroxyl T_1 in a spin-labeled porphyrin. *Modern Applications of EPR/ESR: From Biophysics to Materials Science, Proceedings of the Asia-Pacific EPR/ESR Symposium, 1st, Kowloon, Hong Kong, Jan. 20–24, 1997*. 19–24.

44. Fielding, A. J., D. B. Back, M. Engler, B. Baruah, D. C. Crans, G. R. Eaton, and S. S. Eaton. 2007. Electron spin lattice relaxation of V(IV) complexes in glassy solutions between 15 and 70 K. *ACS Symp. Ser.* 974:364–375.

45. Fielding, A. J., S. Fox, G. L. Millhauser, M. Chattopadhyay, P. M. H. Kroneck, G. Fritz, G. R. Eaton, and S. S. Eaton. 2006. Electron spin relaxation of copper(II) complexes in glassy solution between 10 and 120 K. *J. Magn. Reson.* 179:92–104.

46. Eaton, S. S., and G. R. Eaton. 2000. Relaxation times of organic radicals and transition metal ions. *In* Distance Measurements in Biological Systems by EPR. L. J. Berliner, S. S. Eaton, and G. R. Eaton, editors. Kluwer Academic/Plenum Publishers, New York. 29–154.

47. Poole, C. P., and H. Farach. 1971. Relaxation in Magnetic Resonance. Academic Press, New York.

48. Kulikov, A. V., and G. I. Likhtenshtein. 1977. The use of spin relaxation phenomena in the investigation of the structure of model and biological systems by the method of spin labels. *Adv. Mol. Relax. Interact. Proc.* 10:47–69.

49. Salikhov, K. M., and Y. D. Tsvetkov. 1979. Electron spin-echo studies of interactions in solids. *In* Time Domain Electron Spin Resonance. L. Kevan and R. N. Schwartz, editors. John Wiley, New York. 232–277.

50. Zhidomirov, G. M., and K. M. Salikhov. 1969. Contribution to the theory of spectral diffusion in magnetically diluted solids. *Sov. Phys. JETP*. 29:1037–1040.

51. Brown, I. M. 1979. Electron spin echo studies of relaxation processes in molecular solids. *In* Time Domain Electron Spin Resonance. L. Kevan and R. N. Schwartz, editors. John Wiley, New York. 195–229.

52. Zecevic, A., G. R. Eaton, S. S. Eaton, and M. Lindgren. 1998. Dephasing of electron spin echoes for nitroxyl radicals in glassy solvents by non-methyl and methyl protons. *Mol. Phys.* 95:1255–1263.

53. Arnold, E. V., D. S. Bohle, and P. A. Jordan. 1999. Reversible and irreversible hemichrome generation by the oxygenation of nitrosylmyoglobin. *Biochemistry.* 38:4750–4756.

54. Peisach, J., and W. B. Mims. 1977. Linear electric field effect in electron paramagnetic resonance for two bisimidazole-heme complexes, model compounds for B and H hemichromes of hemoglobin and for cytochrome *b5*. *Biochemistry.* 16:2795–2799.

55. Kay, M. S., C. H. Ramos, and R. L. Baldwin. 1999. Specificity of native-like interhelical hydrophobic contacts in the apomyoglobin intermediate. *Proc. Natl. Acad. Sci. USA*. 96:2007–2012.

56. Scott, E. E., E. V. Paster, and J. S. Olson. 2000. The stabilities of mammalian apomyoglobins vary over a 600-fold range and can be enhanced by comparative mutagenesis. *J. Biol. Chem.* 275:27129–27136.

57. Barrick, D., and F. W. Dahlquist. 2000. *Trans*-substitution of the proximal hydrogen bond in myoglobin: I. Structural consequences of hydrogen bond deletion. *Proteins Struct. Funct. Genet.* 39:278–290.

58. Langen, R., K. J. Oh, D. Cascio, and W. L. Hubbell. 2000. Crystal structure of spin labeled T4 lysozyme mutants: implications for the interpretation of EPR spectra in terms of structure. *Biochemistry.* 39:8396–8405.

59. Kispert, L. D., M. K. Bowman, J. R. Norris, and M. S. Brown. 1982. Electron spin echo studies of the internal motion of radicals in crystals: phase memory vs. correlation time. *J. Chem. Phys.* 76:26–30.

60. Eaton, S. S., and G. R. Eaton. 2000. Distance measurements by CW and pulsed EPR. *Biol. Magn. Reson.* 19:1–27.

61. Baldwin, R. L. 1995. Alpha-helix formation by peptides of defined sequence. *Biophys. Chem.* 55:127–135.

62. Cavagnero, S., Y. Theriault, S. S. Narula, H. J. Dyson, and P. E. Wright. 2000. Amide proton hydrogen exchange rates for sperm whale myoglobin obtained from 15N–1H NMR spectra. *Protein Sci.* 9:186–193.

63. Feng, Z., M. C. Butler, S. L. Alam, and S. N. Loh. 2001. On the nature of conformational openings: native and unfolded-state hydrogen and thiol-disulfide exchange studies of ferric aquomoglobin. *J. Mol. Biol.* 314:153–166.

64. Poole, C. P., Jr., and H. A. Farach. 1971. Dipolar interaction. *In* Relaxation in Magnetic Resonance. C. P. Poole, Jr., and H. A. Farach, editors. Academic Press, New York. 69–71. Eqs. 66.42–66.44.